Materials Science and Engineering A352 (2003) 232–239

Impedance spectroscopy of a soda-lime glass during sintering

R. Muccillo [a,*], E.N.S. Muccillo [a], Y.V. França [a], C. Fredericci [b], M.O. Prado [b], E.D. Zanotto [b]

[a] *Centro Multidisciplinar para o Desenvolvimento de Materiais Cerâmicos, CCTM-Instituto de Pesquisas Energéticas e Nucleares, C.P. 11049, Pinheiros, São Paulo, SP 05422-970, Brazil*

[b] *Departamento de Engenharia de Materiais, Universidade Federal de S. Carlos, C.P. 676, São Carlos, SP 13.565-905, Brazil*

Received 30 July 2002; received in revised form 15 November 2002

Abstract

Impedance spectroscopy measurements were carried out during sintering of a compact of spherical soda-lime-silica glass particles (SiO_2 72.5 wt.%, MgO 3.3%, CaO 9.8%, Na_2O 13.7%, Al_2O_3 0.4%, Fe_2O_3 0.2%, K_2O 0.1%). Impedance diagrams were obtained in the 5 Hz–13 MHz frequency range at different temperatures during room temperature −943 K–room temperature cycles. The glass transition temperature evaluated using the total electrical resistance of the glass specimens agrees with the value obtained by differential scanning calorimetry. The electrical conductance increases with the time that the glass is maintained at the sintering temperature suggesting that this behavior may be used to the study of sintering kinetics. A model to gather information on the sintering kinetics from conductivity data was developed and tested.

Keywords: Glass sintering; Impedance spectroscopy; Soda-lime glass; Sintering modelling

1. Introduction

The impedance spectroscopy (IS) technique consists in the measurement of the electrical impedance Z as a function of the frequency of the input signal over a wide frequency range. The collected data may be visualized as a Nyquist diagram, represented by the imaginary component Z'' of the impedance as a function of Z', the real component. Different contributions to the resistivity of a solid material due to phases with different resistivity, as for example grain and grain boundaries in solid electrolytes, may be separated in the frequency domain using that technique [1–3]. The main parameters that are determined by the IS technique are the electrical resistance, the characteristic relaxation time and the decentralization angle ϕ of each component of the system. An important aspect of the IS technique is that there is often a relationship between the behavior of real systems and that of an idealized electrical circuit consisting of association of discrete electrical components. Impedance data are, therefore, compared or fitted to an equivalent circuit which is representative of the transport phenomena taking place in the system under investigation.

Since 1973 the IS technique has been used to study the electrical behavior of glasses [4]. Several reports on the application of that technique to the study of glasses have been reported afterwards [5–20]. All those references have one common point: they deal with consolidated glass specimens, namely, the IS technique has been used in glass samples *after* preparation through mixing and melting. In this paper, the IS measurements have been carried out *during* sintering.

The crystallization of a Li-disilicate glass was also analyzed by the IS technique [21]. A model was developed to analyze the evolution of the electrical conductivity during glass crystallization, in the case where one phase (Li-disilicate crystals) has an electrical conductivity several orders of magnitude lower than that of the glassy phase. Beyond the percolation limit (the content of the high conductivity phase that leads to a sudden increase in the system conductivity with an increase of this phase), that model was conceived using a

* Corresponding author. Tel./fax: +55-11-3816-9343.
E-mail addresses: muccillo@usp.br (R. Muccillo), dedz@power.ufscar.br (E.D. Zanotto).

0921-5093/02/$ - see front matter
PII: S0921-5093(02)00893-6

power law for the electrical conductivity and the Johnson–Mehl–Avrami theory to take into account the volume crystallization rate. The experimental data was analyzed within the framework of that model [21].

In the system here studied, pores have an electrical conductivity several orders of magnitude lower than that of the glass, its electrical behavior being similar to the reported crystal–glass system [21]. A model with an electrical conductivity described by a power law was then developed, since the microstructure of our system is well beyond the percolation limit. The percolation limit is reached at $\sim$16% of the total space filled by the glass spheres, while in our experiments the occupancy is $\sim$ 60% of the total space even before sintering starts.

The evolution of the samples density during sintering is computed using the Clusters model [22–24], resulting in equations that predict the evolution of the electrical conductivity during sintering of a glassy porous body. Although the glass used in this work partially devitrifies during sintering [23], due to crystallization from the particle surfaces, the crystallized fraction is negligible at the experimental temperatures and sintering times. Thus the contribution of the crystal phases to the electrical conductivity are not considered.

A complicating experimental factor is the pressure applied by the electrodes on the samples during sintering. This pressure puts the samples under compression that deforms it by viscous flow, thus influencing the electrical resistance. This last effect is included in our calculations.

There are reports on IS measurements on ceramic specimens during sintering [25,26], but to the best of our knowledge, IS results on glass sintering are here reported for the first time.

2. Experimental

Spherical soda-lime-silica glass particles (SiO_2 72.5wt.%, MgO 3.3%, CaO 9.8%, Na_2O 13.7%, Al_2O_3 0.4%, Fe_2O_3 0.2%, K_2O 0.1%) with diameter within 80–70 mesh were only slightly pre-sintered in an alumina crucible to cylindrical pellets with a relative density of 0.61. The pellets were inserted in a high temperature sample chamber, having platinum terminal leads to the impedance analyzer. The electrical measurements were then taken at several temperature dwellings during heating from room temperature to a temperature closely below the glass softening temperature, and also during cooling down to room temperature. Electrical measurements were also performed on samples aged for cumulative periods of time at 943 K. The samples were inserted between platinum disks into an alumina holder and positioned (spring-loaded) inside a tubular furnace. Platinum leads connected the platinum disks to an HP4192A LF Impedance Analyzer controlled by a model 362 Hewlett Packard Controller for collecting, storing and processing ($-Z'' \times Z'$) data in the 5 Hz–13 MHz frequency range. A special software was used for that purpose [27]. The applied voltage signal amplitude was 100 mV. A S-type thermocouple with its tip located close to the sample was used for temperature monitoring. The temperature cycling was the following: 10 °C min^{-1} heating rate up to approximately 700 °C and down to room temperature, stopping for data collection (16 frequencies per decade with a 5 s delay between each voltage input excitation) in 10° steps for 6 min. Data were also collected as a function of the time the specimen was kept at a temperature close to the softening temperature.

Differential Scanning Calorimetry measurements were performed in a STA 409 Netzsch Simultaneous Thermal Analysis equipment. The analyses were carried out at 10° C min^{-1} under a flow of pure argon gas.

3. Results and discussion

Fig. 1 shows Arrhenius plots of the electrical resistance of the glass specimen from room temperature to 943 K and back to room temperature. The values in the Arrhenius plot are the total electrical resistance values determined at the intersection of the semicircles with the x-axis in the low frequency region. A set of some of the IS diagrams measured in the same temperature cycle is shown in Fig. 2a–h. These figures show the actual impedance diagrams at the indicated temperatures pointed by the arrows in Fig. 1. At the beginning of sintering the impedance diagrams consist usually of a single semicircular arc showing the high resistance of the pressed glass spheres. The system under measurement consists on touching glass spheres and pores. Later, as sintering proceeds and the glass specimen solid body consolidates, a better defined semicircular arc at higher frequencies and an inclined spike in the lower frequencies region are detected. For increasing temperatures, the high frequency semicircle arc decreases while the low frequency spike increases. Such behavior is typical of ion conducting solids with blocking electrodes. The high frequency arc is representative of the bulk properties and the response at lower frequencies is representative of the electrode polarization [4]. The main features of the impedance diagrams are: (1) the electrical resistance of the glass specimens during sintering (heating up from RT upwards) are higher than the resistance of the corresponding temperatures during cooling down the sintered glass specimens. This is due to the fact that during sintering two are the contributions to the resistivity, namely, one due to the glass spheres and other due to the pores in the space between them. During cooling the sintered specimens, there should be only one contribution due to the glass spheres because it

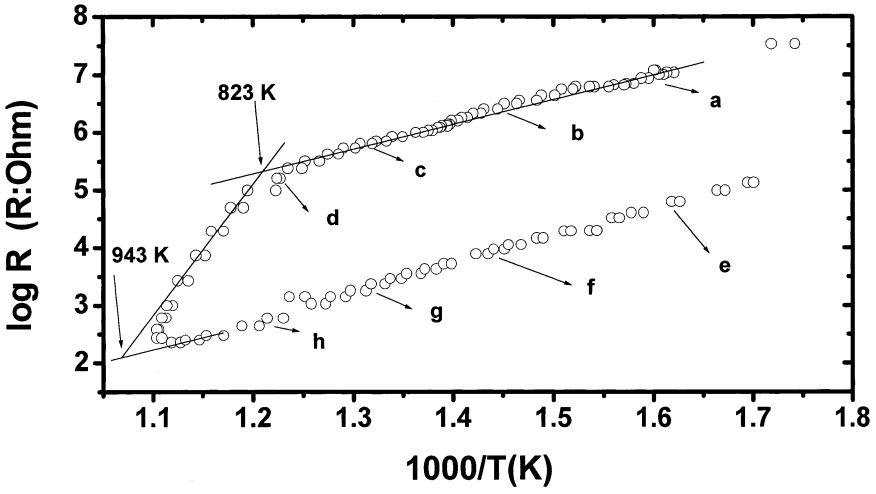

Fig. 1. Arrhenius plots of the total electrical resistance of packed spheres of soda-lime-silica glass from room temperature to 943 K and back to room temperature. Arrows refer to Fig. 2.

is expected that the pores be mostly excluded after the specimen reaches higher density. (2) The semicircles of the impedance diagrams measured below the softening temperature are skewed, with their centers lying below the x-axis. For temperatures lower than the softening temperature, after the glass specimen is sintered, the semicircles have their centers very close to the x-axis, i.e., the decentralization angle is approximately zero. The apparent higher than zero decentralization angle in the first impedance diagrams after the specimen reaches the softening temperature is due to an inductance effect known to occur in the high frequency/low resistance region of the impedance analyzer. After making the proper correction of that inductance effect, a close to zero decentralization angle is obtained. The reason the decentralization angles are different in the impedance diagrams taken before (heating up) and after (cooling down) the specimen reaches 943 K is that this angle reflects the degree of homogeneity of the glass specimen. During the heating from RT up to 943 K, the specimen is composed of glass spheres and pores; after 943 K is reached, the glass specimen presents lower values of electrical resistance due to the reduction of porosity and, consequently a higher degree of homogeneity with the glass spheres collapsing to form a more dense body.

Let us now analyze the Arrhenius plots. The first observation is that the straight lines obtained during heating up and during cooling down are parallel. This usually means that the charge carriers responsible for the transport phenomenon being measured (electrons, holes or ions) are the same all over both temperature cycles.

The glass transition (T_g) temperature can be determined after the Arrhenius plots: when heating up the glass specimen from room temperature, the slope of the straight line increases abruptly at T_g. We assume that at this point the glass reaches the transition temperature, determined as 550 °C, in agreement with DSC experiments.

Another experiment was performed as an attempt to follow the sintering kinetics: a slightly sintered pellet of spherical soda-lime-silica glass particles was inserted into the sample chamber, which was then inserted in the tubular furnace, which was set to the following temperature profile: fast (30° min^{-1}) heating up to 943 K, keeping at that temperature for 15 min, cooling down to 653 K for the IS measurement, heating up at 30° min^{-1} to 943 K for another 15 min, and so on. The IS data were then taken after the specimen is kept at regular time intervals at 943 K. In this way the kinetics of sintering at 943 K is monitored by determining the total electrical resistance of the IS data. The IS data were not measured at 943 K due to limitations of the impedance analyzer. At that temperature the resistance of the glass specimen is smaller than the minimum detectable resistance. The idea behind this experiment was to follow the sintering of a glass specimen using the IS technique. Another technique, the determination of the apparent density, had been used by some of the authors of this paper to follow densification and to check a model they proposed for sintering polydispersed glass particles [22].

The results are shown in Fig. 3 where the reciprocal of the total electrical resistance is plotted as a function of the time that the specimen is kept at 943 K.

The impedance diagrams are similar to the ones shown in Fig. 2, having two components: a semicircular arc and a spike. The values of the total electrical resistance were determined after deconvolution of the components of each impedance diagram ($-\mathrm{Im}\ Z \times \mathrm{Re}\ Z$), by the intercept of the high frequency semicircle arc with the x-axis far from the axis origin with the real axis.

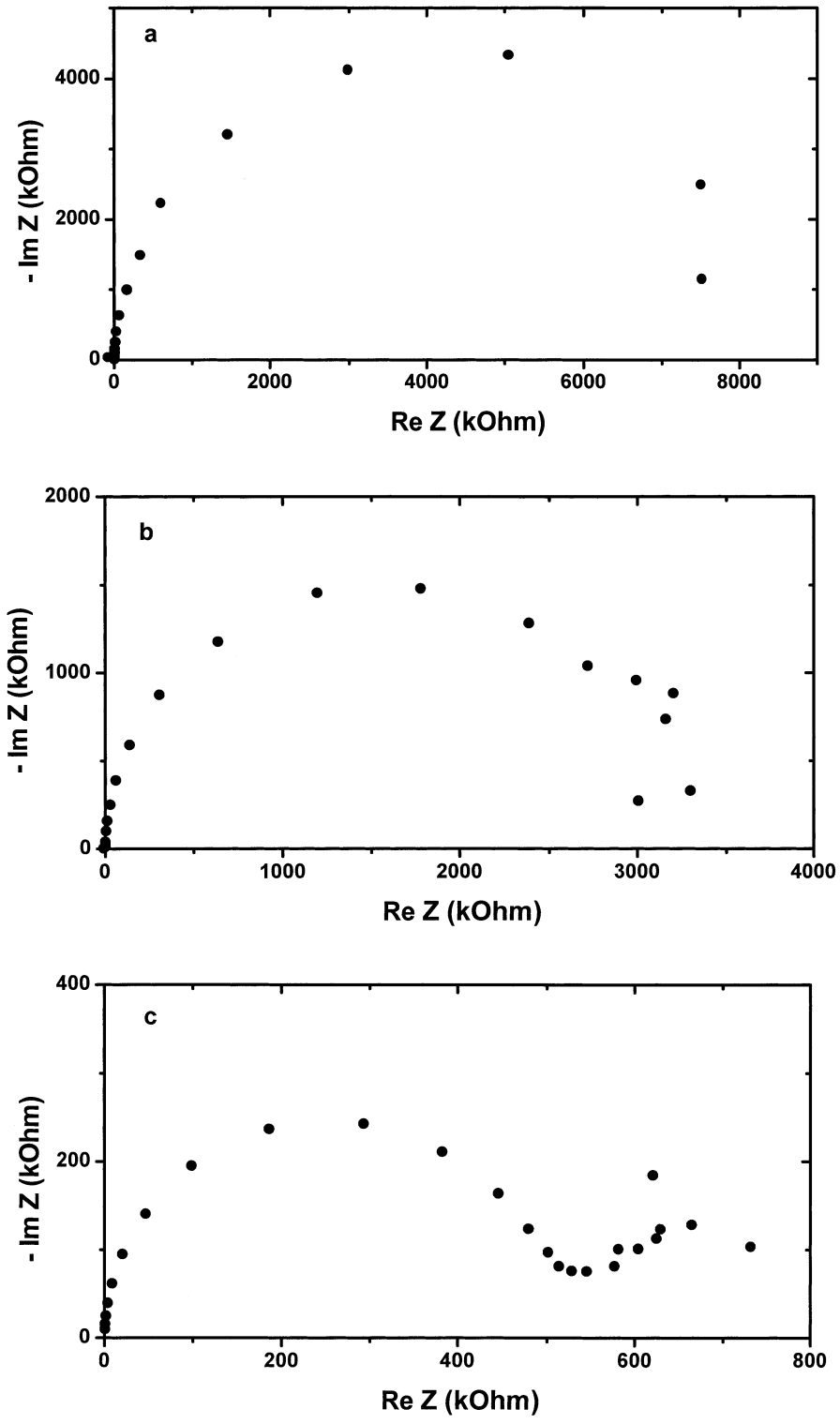

Fig. 2. IS diagrams of packed spheres of soda-lime-silica glass at different temperatures during heating (a, b, c and d) and cooling (e, f, g and h). Arrows in Fig. 1 point the temperatures the diagrams were obtained.

Plotting these values, determined from the IS diagrams, as a function of the time that the glass specimen is maintained at a particular temperature is here proposed as an alternative way to follow the kinetics of sintering.

3.1. Electrical conductivity evolution during isothermal sintering of glass particles: a simple model

In this section we provide an explanation for the correlation between electrical conductivity and isother-

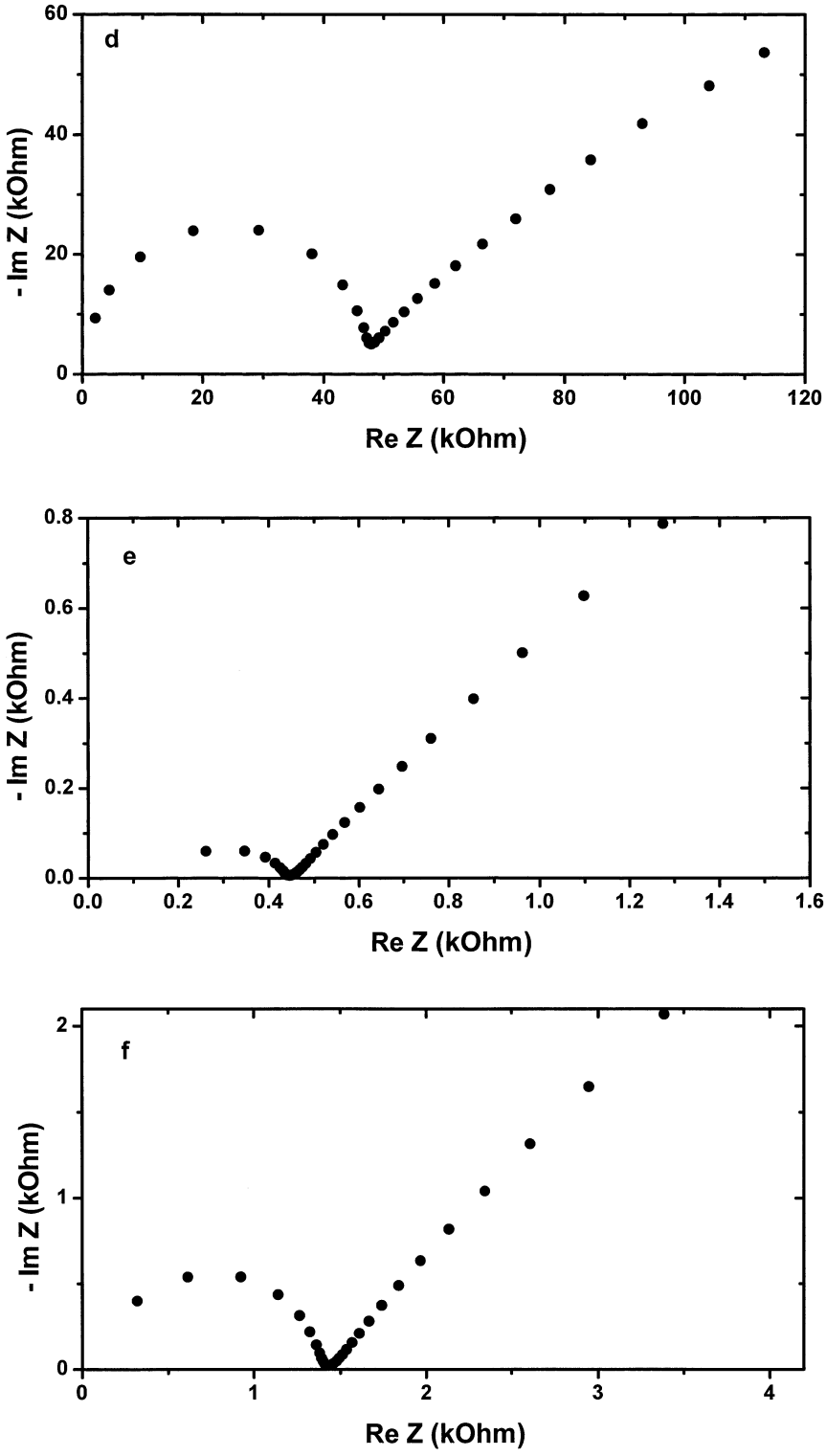

Fig. 2 (*Continued*)

mal densification of glass compacts. During sintering, two concurrent phenomena are responsible for changes in the electrical resistance of the sample (a compact of glass particles). First, changes in the sample dimensions due to sintering shrinkage with concurrent reduction of porosity, in this case, assisted by the pressure of the spring load system of the electrodes; and second, viscous deformation of the glass due to the same load.

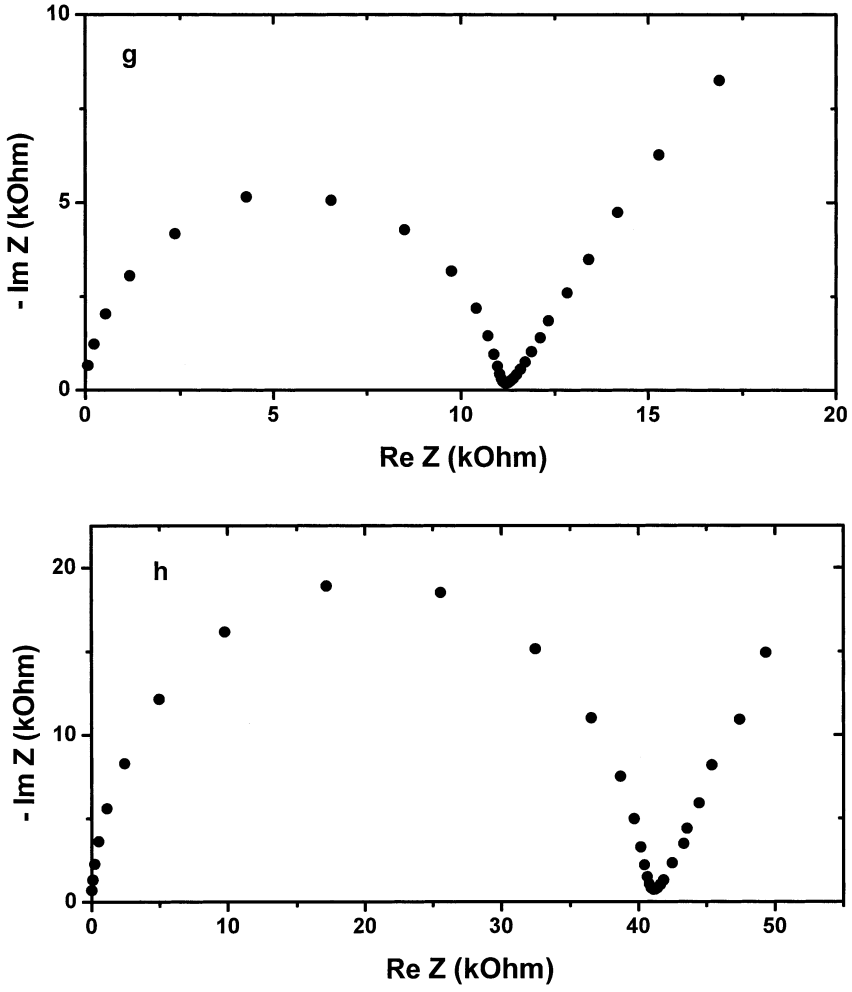

Fig. 2 (*Continued*)

Let us see how one can calculate the expected electrical resistance during an isothermal sintering experiment at a temperature T, and then compare the expected values with the measured ones.

3.2. Shrinkage due to the sintering under applied pressure

Let us define σ_g and $\sigma(t)$ as the intrinsic conductivity of the glass (without porosity) and the porous compact

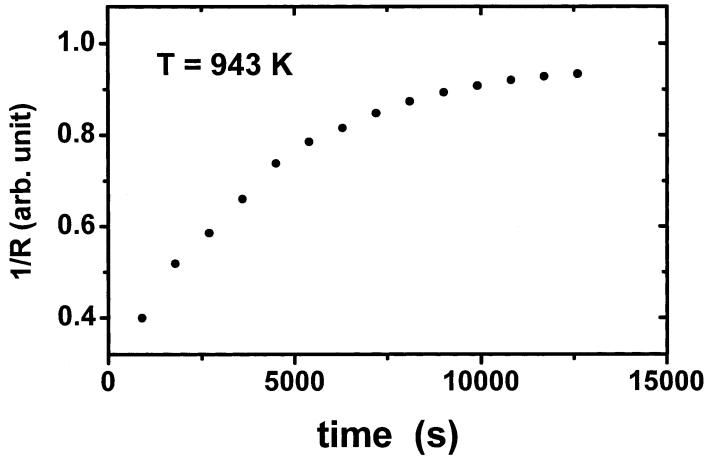

Fig. 3. Dependence of the electrical conductance of packed spheres of soda-lime-silica glass on the time the specimen is maintained at 943 K. Temperature of measurements: 653 K.

conductivity at time t, respectively; δ_0 and $\delta(t)$ the relative green density (with respect to the glass density) of the sample before sintering and at time t. $l(0)$ and $r(0)$ are the cylindrical sample height and radius at time = 0. Then, from the model of Kanert et al. [21], the electrical conductivity and resistivity of the porous body are given by Eq. (1) [21].

$$\sigma(t) = \sigma_g(\delta(t) - \delta_c)^{\gamma} \qquad R(t) = \sigma(t)^{-1}\frac{l(t)}{\pi r(t)^2} \tag{1}$$

where δ_c is the electrical conductivity percolation limit ($0.1 < \delta_c < 0.3$), below which the electrical properties are governed by pores, and γ is a constant having a value between 1.3 and 1.7. However, in our case $\delta(t) \geqslant \delta_0 = 0.6 \gg \delta$.

The evolution of density with time, $\delta(t)$ in Eq. (1), can be calculated using the Clusters model [22–24]:

$$\delta(t) = \delta_0 \frac{1}{(1 - \Delta r(t))^2(1 - \Delta l(t))} \tag{2}$$

From Eq. (2) the linear shrinkage of the sample can be derived. In deriving Eq. (2) the shrinkage anisotropy of the sample was considered. Anisotropy was caused by the spring load system of the electric contacts. The radial shrinkage with time (normalized to $r(0) - \Delta r(t)$) was smaller than the height shrinkage with time (normalized to $l(0) - \Delta l(t)$).

For isotropic sintering conditions:

$$\delta(t) = \delta_0 \frac{1}{(1 - \Delta l(t))^3} \quad \text{thus} \quad \Delta l(t) = 1 - \left(\frac{\delta_0}{\delta(t)}\right)^3 \tag{3}$$

Δl was calculated from Eq. (3), computing $\delta(t)$ with the Clusters model for sintering, with an applied pressure. Δr was calculated in the same way, but without applied pressure.

3.3. Viscous deformation

The axial linear deformation, Δl_p, of a glass cylinder subjected to an axial pressure $p = mg/(\pi r_0^2)$ (mg is the load applied on the circular area πr_0^2) is given by Eq. (4) [28]

$$\Delta l_p = \frac{pl\Delta t}{3\eta} \tag{4}$$

where Δt is the time under load and η is the glass viscosity.

Since the compact under study started with a green density of 0.61, which increased with time,

$$\Delta l_p = \frac{pl\Delta t}{3\eta}\int_0^t \frac{dt'}{\rho(t')} \tag{5}$$

Despite the deformation the sample volume remains constant. If Δr_p is the radial increase due to deformation caused by the applied pressure, then:

$$[1 - \Delta r_p(t)]^2[1 - \Delta l_p(t)] = 1 \tag{6}$$

Including in the expression of the electrical resistance Eq. (1), the sintering shrinkage (Eqs. (2) and (3)), and the sample deformation (Eqs. (5) and (6)), we obtain Eq. (7) for the electrical resistance during sintering with an applied force:

$$\frac{R(0)}{R(t)} = \left[\frac{\delta_0}{(1 - \Delta r(t))^2(1 - \Delta l(t))} - \delta_c\right]^{\gamma} \times \frac{[1 - \Delta r(t)]^2}{[1 - \Delta l_p(t)]^2[1 - \Delta l(t)][\delta_0 - \delta_c]^{\gamma}} \tag{7}$$

By means of the Clusters model, we estimated that sintering on the 943–673–943 K heating/cooling path, between each sequential isothermal sintering at 943 K, was negligible. The compact's density increased only about 1/1000 in each measurement cycle.

Fig. 4 compares the plots of measured and computed values of $(R(0)/R(t))$ vs. time. The electrical resistance changes during sintering follows a similar trend as the calculated changes due to sintering. The spring load system applies a force on the porous body, and the deformation of the pores (that are not considered in the calculations) may cause the mismatch between the measured and computed values.

4. Conclusions

The IS technique can be used to study the sintering of glass compacts. A model developed in this work allows to gather information on the sintering kinetics from electrical conductivity data. With this technique the densification kinetics can be monitored after deconvolution of the impedance diagrams measured isothermally as a function of time. However, further research work is

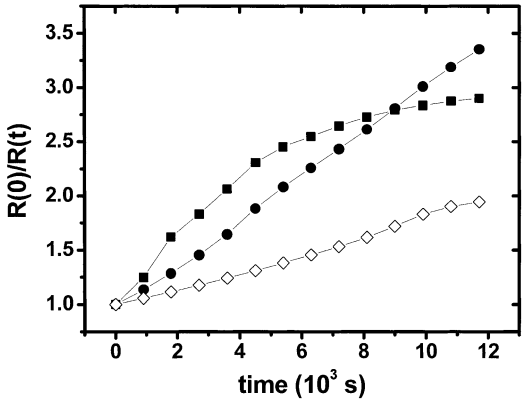

Fig. 4. $R(0)/R(t)$ estimated with the model leading to Eq. (7). Hollow diamonds: without applied pressure; solid circles: applied pressure of 3.5 kPa; solid squares: from electrical resistance measurements.

needed to quantitatively link the density (porosity) and the electrical conductivity of the sample.

Acknowledgements

To A.C.M. Rodrigues and Q. Uhm for critical comments. To CNEN, CNPq, PRONEX, FAPESP (99/10798-0 and 99/00871-2) for financial support.

References

[1] J.E. Bauerle, J. Phys. Chem. Sol. 30 (1969) 2657.
[2] M. Kleitz, H. Bernard, E. Fernandez, E Schouler, in: A.H. Heuer, L.W. Hobbs (Eds.), Science and Technology of Zirconia I, Advances in Ceramics, vol. 3, The American Ceramic Society, Columbus, OH, 1981, p. 310.
[3] I.D. Raistrick, in: J.R. Macdonald (Ed.), Impedance Spectroscopy-Emphasizing Solid Materials and Systems, Wiley Interscience, New York, 1987, p. 29.
[4] D. Ravaine, J.L. Souquet, J. Chim. Phys. 71 (1973) 693.
[5] M. Audier, D. Ravaine, J.L. Souquet, C.R. Acad. Sci. Paris, t. 282, s. C (1976) 499.
[6] D. Ravaine, J.L. Souquet, Phys. Chem. Glasses 18 (2) (1977) 27.
[7] M. Ribes, B. Barrau, J.L. Souquet, J. Non-Cryst. Sol. 38&39 (1980) 271.
[8] H.L. Downing, N.L. Peterson, H. Jain, J. Non-Cryst. Sol. 50 (1982) 203.
[9] E. Robinel, B. Carette, M. Ribes, J. Non-Cryst. Sol. 57 (1983) 49.
[10] E. Robinel, A. Kone, M.J. Duclot, J.L. Souquet, J. Non-Cryst. Sol. 57 (1983) 59.
[11] J.M. Hyde, M. Tomozawa, M. Yoshiyagawa, Phys. Chem. Glasses 28 (5) (1987) 175.
[12] M. Tomozawa, J.M. Hyde, J.F. Cordaro, M. Yoshiyagawa, Phys. Chem. Glasses 33 (3) (1992) 69.
[13] P. Dzwonkowski, M. Eddrief, C. Julien, M. Balkanski, Mater. Sci. Eng. B8 (1991) 193.
[14] B. Wang, S.P. Szu, M. Greenblatt, J. Non-Cryst. Sol. 134 (1991) 249.
[15] B.V.R. Chowdary, K.F. Mok, J.M. Xie, R. Gopalakrishnan, J. Non-Cryst. Sol. 160 (1993) 73.
[16] J.R. Min, J. Wang, L.Q. Chen, R.J. Xue, W.Q. Cui, J.K. Liang, Phys. Stat. Sol. (a) 148 (1995) 383.
[17] K.C. Sobha, K.J. Rao, J. Non-Cryst. Sol. 201 (1996) 52.
[18] B. Munro, B. Wang, M. Greenblatt, J. Non-Cryst. Sol. 196 (1996) 291.
[19] K. El-Egili, J. Phys.: Condens. Matter 8 (1996) 3419.
[20] R.F. Bartholomew, D.M. Young, A.J.G. Ellison, J. Non-Cryst. Sol. 256&257 (1999) 242.
[21] O. Kanert, P. Küchler, D. Suter, G.N. Shanon, H. Jain, J. Non-Cryst. Sol. 274 (2000) 202.
[22] M.O. Prado, E.D. Zanotto, R. Müller, J. Non-Cryst. Sol. 279 (2001) 169.
[23] E.D. Zanotto, M.O. Prado, Phys. Chem. Glasses 42 (3) (2001) 191.
[24] M.O. Prado, C. Fredericci, E.D. Zanotto, Phys. Chem. Glasses, 43 (5) (2002).
[25] R. Muccillo, J.A. Cerri, E.R. Leite, E. Longo, J.A. Varela, Mater. Lett. 30 (1997) 125.
[26] D.Z. de Florio, R. Muccillo, Sol. State Ionics 123 (1–4) (1999) 301.
[27] M. Kleitz, J.H. Kennedy, in: P. Vashishta, J.N. Mundy, G.K. Shenoy (Eds.), Fast Ion Transport in Solids, Elsevier North Holland, Amsterdam, 1979, p. 185.
[28] J.M. Fernandez Navarro, El vidrio, Instituto de Ceramica y Vidrio, Madrid, 1985, p. 357.